LIMNOLOGY and OCEANOGRAPHY

ASLO

Limnol. Oceanogr. 9999, 2025, 1–15

doi: 10.1002/lno.70227

RESEARCH ARTICLE

Light attenuation due to preferential orientation of particles in waves and shear flow: Idealized modeling for bacteria, algae, and microplastics

Samuel T. Salemink-Harry [1*], **Benjamin J. Smith** [2], **Hilary A. Dugan** [3], **Jennifer A. Franck** [2], **Till J.W. Wagner** [4], **Lucas K. Zoet** [5], **Grace M. Wilkinson** [3], **Nimish Pujara** [1,6]

[1]Department of Civil and Environmental Engineering, University of Wisconsin–Madison, Madison, Wisconsin, USA; [2]Department of Mechanical Engineering, University of Wisconsin–Madison, Madison, Wisconsin, USA; [3]Center for Limnology, University of Wisconsin–Madison, Madison, Wisconsin, USA; [4]Department of Atmospheric and Oceanic Sciences, University of Wisconsin–Madison, Madison, Wisconsin, USA; [5]Department of Geoscience, University of Wisconsin–Madison, Madison, Wisconsin, USA; [6]Department of Civil Engineering, The University of British Columbia, Vancouver, British Columbia, Canada

Abstract

Particles are a key component of aquatic light climate due to their attenuation of light. Near the water surface, waves and sheared currents can induce a preferential orientation of nonspherical particles that alters their inherent optical properties and the associated light attenuation. This modeling study focuses on how particle shape, and the corresponding preferential orientation, impacts the light climate in an aquatic environment. We assume aquatic particles, such as bacteria, algae, and microplastic pollutants, are optically homogeneous spheroids that move with the flow. The model computes their preferential orientations within the upper water column in flow driven by linear water waves and sheared currents. This is combined with the anomalous diffraction optical approximation to examine the effect of particle orientation on the beam attenuation coefficient. We find that the preferential orientation by waves and shear tends to increase the projected area of the spheroid compared to random (isotropic) orientation. This has particle size-dependent effects on light attenuation: for particles comparable in size and shape to algae or microplastics, the preferential orientation corresponds to an increase of 10–25% in the beam attenuation coefficient, whereas there is a decrease of 10–20% in the beam attenuation coefficient for smaller particles comparable in size to bacteria. Overall, our results reveal how preferential orientation of nonspherical particles by waves and currents can impact light climate in the upper water column.

The underwater light climate is critical for aquatic ecosystems, where photosynthetic organisms compete for light near the water surface and occlude light beneath them. Aquatic organisms and particles, along with the water itself and any organic or inorganic compounds, influence the bulk optical properties of the water column such as absorption, scattering, attenuation, and fluorescence (Rose 2024). These optical properties are routinely used to estimate the concentration of dissolved and particulate constituents in the water column, such as dissolved organic carbon or phytoplankton biomass, via in situ methods (Bricaud et al. 2004; Nayak et al. 2021) and remote sensing (Ross et al. 2019; Werdell et al. 2018). The optical properties also modify the underwater light field of the water column, resulting in partially polarized light that loses intensity with depth (Lehmuskero et al. 2018).

How particles in a water column modify the light field depends on the wavelength of light as well as the composition, size, shape, and concentration of the particles. While optical models used in natural aquatic environments frequently assume uniformly random (isotropic) particle orientations (Clavano et al. 2007; Jonasz and Fournier 2007), particle optical properties are in fact strongly influenced by orientation (Mishchenko et al. 2002), so much so that optical

*Correspondence: sam.saleminkharry@wisc.edu

Associate editor: David Antoine

measurements are routinely used to determine particle orientation (Font-Muñoz et al. 2020; Noel and Chepfer 2004; Seo et al. 2014). Furthermore, it has been shown in the laboratory and the field that oceanic shear flows can alter light attenuation by causing preferential alignment of bacteria and phytoplankton (Marcos et al. 2011; McFarland et al. 2020). Since flow-induced orientations influence the light availability in the water column, our main objective in this paper is to investigate how the preferential alignment caused by the combined effect of waves and shear flows influences light attenuation in the upper water column.

Flow-induced re-orientations of idealized particles that are small, neutrally buoyant ellipsoids are frequently modeled using Jeffery's (1922) equations. Under this framework, different flow conditions have been found to induce different patterns of preferential particle orientations. For example, homogeneous turbulence far from walls causes the longest particle axis to align with the fluid vorticity, whereas near-wall turbulence aligns the longest particle axis in the flow (wall-parallel) direction (Pujara et al. 2021; Voth and Soldati 2017; Zhao and Andersson 2016). In many natural aquatic environments, the flow near the water surface is dominated by a combination of water waves and surface currents where the preferential orientation of particles follows well-described patterns (DiBenedetto et al. 2017; DiBenedetto and Ouellette 2018; Ma et al. 2022; Pujara and Thiffeault 2023; Ventrella et al. 2023). In this paper, we investigate the consequences of these preferential particle orientation patterns on light attenuation in the water column.

To reduce the scope of the optical problem, we consider an idealized case of monochromatic, unpolarized light attenuation by optically homogeneous spheroid particles in the water column. The attenuation by the water itself or other components is neglected. The light is both scattered and absorbed by the particles: scattered light is redirected, and absorbed light is converted to another form of energy. The resulting attenuation, also called extinction, is the sum of scattering and absorption. For simplicity, we neglect that each particle is exposed to light scattered by other particles. These simplifying assumptions restrict our analysis to the beam attenuation coefficient that describes the attenuation of a narrow, collimated beam of light (e.g., Mobley et al. 2020). To isolate the influence of orientation, we consider the case where particles have uniform size and shape and compare the flow-aligned light attenuation to that assuming uniformly random orientation.

Since aquatic particles vary greatly in size, shape, and composition, we follow Clavano et al. (2007) in the selection of representative values. Organic aquatic particles can range from bacteria on the scale of 1 μm to diatom colonies with length scales on the order of 1 mm, while inorganic particles similarly range from small clay-like particles on the scale of 0.5 μm to microplastics on the order of 5 mm (Cózar et al. 2014; Stramski et al. 2004). In addition, particle shape can vary greatly between aquatic particles: organic particles tend to be prolate in shape (i.e., long and narrow), whereas inorganic particles, such as sediments and microplastics, vary more broadly between prolate and oblate (i.e., wide and flat) (Bickmore et al. 2002; Contreras et al. 2024). Furthermore, the refractive index also varies between organic and inorganic particles (Clavano et al. 2007). We consider two representative values of the refractive index of particles grouped by organic and inorganic while examining the effect of size, shape, and orientation on the beam attenuation coefficient by a given particle type.

We examine idealized particles representing those commonly found near the water surface. For organic particles, these are bacteria or algae. For inorganic particles, these are slightly buoyant plastic particles made of polyethylene, a common microplastic pollutant (Contreras et al. 2024). Furthermore, we restrict our study to the scenario where a single particle type dominates, such as algal blooms where a single species is present in high concentrations (Rose 2024).

In the remainder of the paper, we first establish the background and methodology to analyze the idealized problem outlined above ("Modeling" section). Then, we show our predictions of light attenuation under waves relative to the state of random orientation ("Results" section) and examine how specific aquatic particles change light attenuation ("Applications" section). We end with a review of the main results and a discussion of the model's strengths and weaknesses with suggestions for future research ("Discussion and conclusions" section).

Modeling

Flow induced preferential orientation

We first consider how water waves and wind-driven sheared surface currents affect the orientation of particles in the water column. Our orientation modeling framework, which is illustrated in Fig. 1a follows Pujara and Thiffeault (2023) and Ventrella et al. (2023), uses linear wave theory with a superposed sheared current and models particles as tracer-like spheroids. To produce a tractable model, we neglect complexities arising from several nonlinear aspects, including large wave steepness and wave breaking, inertial effects in flow–particle interactions, and wave–current interactions.

Waves can be described by their period, amplitude, and the water depth over which they propagate. We use linear wave theory (Dean and Dalrymple 1991), in which the wave period, T_w, the wave length, L_w, and the water depth, h, are related by the dispersion relationship $\omega_w^2 = g k_w \tanh(k_w h)$. Here, $\omega_w = 2\pi/T_w$ and $k_w = 2\pi/L_w$ are the angular frequency and wavenumber, respectively; the wave speed is $c_w = L_w/T_w = \omega_w/k_w$, and $g = 9.81$ m s^{-2} is the gravitational acceleration. We focus on the case of deep water relative to the wave length such that $k_w h \to \infty$ ($\tanh(k_w h) \to 1$), in which the dispersion relationship simplifies to $\omega_w^2 = g k_w$. For a given wave amplitude, a_w, the water surface undulation for waves of a single

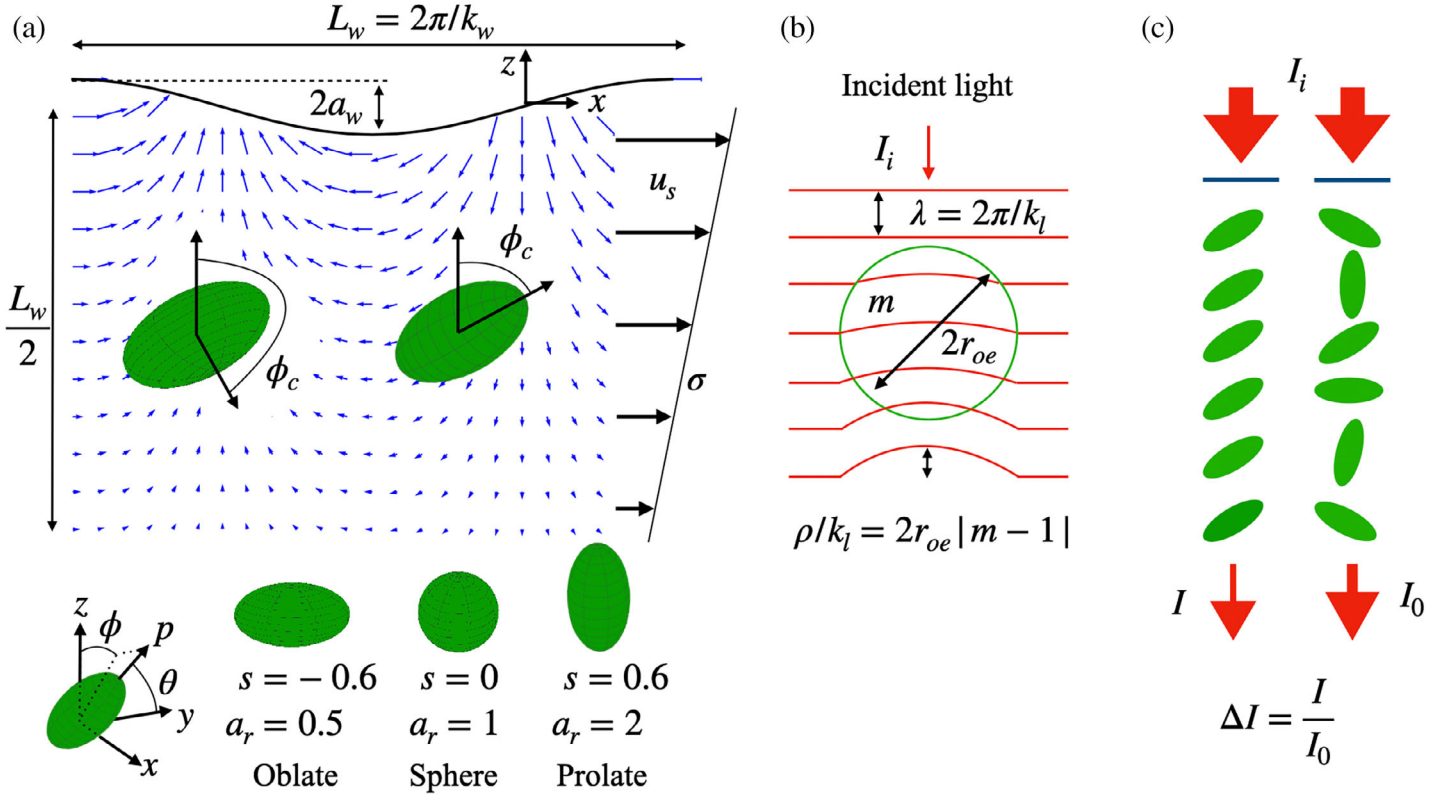

Fig. 1. Model overview: (**a**) preferential orientation of spheroids with various aspect ratios in wave and shear flow, (**b**) optical parameters for light attenuation by a particle, (**c**) change in light attenuation due to preferential particle orientation.

frequency traveling in the positive x direction is given by $\eta = a_w \cos(k_w x - \omega_w t)$ and the corresponding velocity field in the water column is given by $\boldsymbol{u}_w = (u_x, u_z)^T = a_w \omega_w e^{k_w z}(\cos[k_w x - \omega_w t], \sin[k_w x - \omega_w t])^T$ where the superscript T represents the transpose operator. Introducing the dimensionless variables: $t \to \omega_w t$, $\boldsymbol{x} \to k_w \boldsymbol{x}$, and $\boldsymbol{u} \to \boldsymbol{u}/(\omega_w/k_w)$ gives the dimensionless form of the equations where the water surface motion is described by $\eta = \varepsilon \cos(x - t)$ and the corresponding flow velocities given by $\boldsymbol{u}_w = (u_x, u_z)^T = \varepsilon e^z(\cos[x - t], \sin[x - t])^T$. In linear wave theory, the wave steepness, $\varepsilon = k_w a_w$, must remain small, that is, $\varepsilon \lesssim 0.25$.

To include a sheared current, we use the simplest possible model of a linear shear whose interactions with the waves are neglected. The velocity field of the sheared current in dimensionless form is given by $\boldsymbol{u}_s = (\sigma(\xi + z), 0)^T$ where $\sigma = u_s/\xi$ is the shear rate, u_s is the dimensionless current velocity at the surface ($z = 0$), and ξ is the dimensionless depth over which the current exists. Wind generated surface currents tend to be of the order of 0.1 m s^{-1}, but the shear depth varies greatly between water bodies. In the ocean, shear depths are on the order of 100 m (Johnson et al. 2002), with wave periods on the order of 10 s. In contrast, lakes might have shear depths on the order of 1–10 m (Shulman and Bryson 1961; Wu et al. 2018), with wave periods on the order of 1–2 s. The relative scale of shear and waves is comparable, such that in both cases we have $\xi \gtrsim \pi$ and $\sigma \ll 1$.

The equations describing the flow field are given by

$$u_x = \varepsilon e^z \cos(x - t) + \sigma(\xi + z) \tag{1a}$$

$$u_z = \varepsilon e^z \sin(x - t) \tag{1b}$$

and are valid for $-\xi \le z \le 0$. The velocity gradients, $\nabla \boldsymbol{u} = \boldsymbol{S} + \boldsymbol{\Omega}$, in the flow are important for particle orientation where wave motions and shear currents induce strain and rotation in the water column described, with $\boldsymbol{S} = \frac{1}{2}\left(\nabla \boldsymbol{u} + (\nabla \boldsymbol{u})^T\right)$, the strain rate tensor and $\boldsymbol{\Omega} = \frac{1}{2}\left(\nabla \boldsymbol{u} - (\nabla \boldsymbol{u})^T\right)$ the rotation rate tensor. The latter gives the vorticity of the flow and is identically zero for water waves, but nonzero for a sheared current.

We model the effects of rotation and strain on the orientation dynamics of spheroid particles via (Jeffery 1922)

$$\frac{\mathrm{d}\boldsymbol{p}}{\mathrm{d}t} = \boldsymbol{\Omega}\boldsymbol{p} + s(\boldsymbol{S}\boldsymbol{p} - (\boldsymbol{p}^T \boldsymbol{S}\boldsymbol{p})\boldsymbol{p}) \tag{2}$$

where $\boldsymbol{p}$ is the unit vector pointing in the direction of the axis of symmetry of the particle and $s = (a_r^2 - 1)/(a_r^2 + 1)$ is the particle shape factor. Here, $a_r = r_l/r_d$ is the aspect ratio of the spheroid, with r_l the half-length of he particle's symmetry axis, and r_d the particle radius orthogonal to the symmetry

axis (Fig. 1a). The rotation of the particle's symmetry axis by the vorticity is given by $\boldsymbol{\Omega p}$, which is independent of the particle shape. The particle-shape-dependent reorientation due to the strain rate is given by $s\boldsymbol{Sp}$, with $s(\boldsymbol{p}^T\boldsymbol{Sp})\boldsymbol{p}$ ensuring that $\boldsymbol{p}$ remains of unit length. This account of particle reorientation assumes that the particle motion follows the flow and, as such, is relevant for particles that are small and approximately neutrally buoyant.

We extract and expand the orientation component of Ventrella et al. (2023) and analyze the preferential orientation as a function of shear strength, wave steepness, and depth for a neutrally buoyant, non-swimming, inertialess particle. We default to the analysis by Pujara and Thiffeault (2023) in the case of waves without shear.

Ventrella et al. (2023) showed that combining the flow and particle orientation equations with a multi-timescale expansion gives the following wave-averaged orientation dynamics

$$\begin{pmatrix} \frac{\mathrm{d}\phi}{\mathrm{d}t} \\ \frac{\mathrm{d}\theta}{\mathrm{d}t} \end{pmatrix} = s\varepsilon^2 e^{2z} \begin{pmatrix} s+\cos 2\phi \\ \sin 2\phi \sin\theta\cos\theta \end{pmatrix} + \frac{\sigma}{2} \begin{pmatrix} 1+s\cos 2\phi \\ s\sin 2\phi \sin\theta\cos\theta \end{pmatrix} \quad (3)$$

with θ being the polar angle of the particle symmetry axis measured from the y-axis, and ϕ being the angle of the particle symmetry axis in the x–z plane angle measured clockwise from the z-axis (Fig. 1a). In this case, the axis of symmetry is written as $\boldsymbol{p}(\phi,\theta) = (\sin\phi\sin\theta, \cos\theta, \cos\phi\sin\theta)^T$. We refer to ϕ as the zenith angle since it gives the orientation of the particle symmetry axis relative to the optical axis (i.e., the direction of incident light, which is assumed to be vertical).

As previously shown, both with shear (Ventrella et al. 2023) and without (Pujara and Thiffeault 2023), the particles tend to align with the flow plane such that $\theta = \pi/2$. The preferential orientation with the flow plane, quantified by the zenith angle ϕ, may be found from setting the left side of Eq. 3 to zero. This yields the critical zenith angle ϕ_c:

$$\phi_c = \begin{cases} \pi - \phi_0 & a_r < 1 \\ \phi_0 & a_r > 1 \end{cases} \quad (4)$$

where

$$\phi_0 = \frac{1}{2}\arccos\left(-\left[\frac{\sigma + 2s^2\varepsilon^2 e^{2z}}{s(\sigma + 2\varepsilon^2 e^{2z})}\right]\right) \quad (5)$$

This means that there are two different solutions for oblate ($a_r < 1$, $s < 0$) vs. prolate ($a_r > 1$, $s > 0$) spheroids. The critical zenith angle varies with particle shape, shear strength, wave steepness, and depth (Fig. 2).

A critical zenith angle does not always exist: when the influence of the velocity gradient in a sheared current outweighs that due to the wave motions, that is, $s\varepsilon^2 e^{2z} \ll \sigma/2$, the particles undergo periodic rotations known as Jeffery's orbits (Jeffery 1922) following $\mathrm{d}\phi/\mathrm{d}t = (\sigma/2)(1 + s\cos 2\phi)$. This situation, shown by the white regions in Fig. 2, is likely to occur for stronger shear strength (larger σ), smaller aspect ratio (smaller $|s|$), smaller wave steepness (smaller ε), or greater depth (smaller e^{2z}). Since this situation corresponds to no fixed point in the wave-averaged orientation dynamics, a particle orientation distribution would emerge that would be depth-dependent and sensitive to other neglected processes such as rotational diffusion. We avoid this situation here for simplicity and focus on regimes with defined ϕ_c, but note that future work should examine the scenario with nonexistent critical zenith angle.

For purely wave-driven flow ($u_s = \sigma = 0$), the critical zenith angle simplifies to (Pujara and Thiffeault 2023)

$$\phi_0 = \frac{1}{2}\arccos(-s) \quad (6)$$

which does not depend on depth or wave steepness; it is only a function of particle shape (Fig. 3).

Light attenuation

We now consider the attenuation of light by suspended particles in the upper water column with the particles preferentially oriented as described above. Our optical framework follows Shepelevich et al. (2001), where it is assumed that particles are optically soft, optically large, and optically homogeneous spheroids as in the anomalous diffraction (AD) approximation (van de Hulst 1981). Considering monochromatic light and neglecting polarization, we compute the light attenuation (quantified by the beam attenuation coefficient) for particles ranging from bacteria to algae and microplastics.

Light attenuation in lake and ocean water columns can be examined in terms of inherent optical properties (IOPs), which are determined per particle and independent of the incident light, and apparent optical properties (AOPs), which depend on the geometry of the problem. In the field, light attenuation due to suspended particles is estimated via light intensity measurements at multiple depths within a water column that are used to fit to an exponential decay function to infer the diffuse attenuation coefficients, for example, $K(\theta,\phi)$, K_d, or K_{PAR} that are AOPs (see, e.g., Mobley et al. 2020, for more details). Notably, AOPs are difficult to measure in the upper water column due to wave action, meaning that data on the effects of waves on light attenuation are scarce (Rose 2024).

We focus on the interaction of light with suspended particles that can be computed using IOPs. The relevant IOPs for attenuation of unpolarized light are the optical cross sections and the phase function. The optical cross sections describe the amount of light (i.e., radiant flux) that is extinguished, scattered, or absorbed by the particle per incident light intensity (i.e., irradiance). The phase function describes the amount of light scattered by a particle in different directions. For a

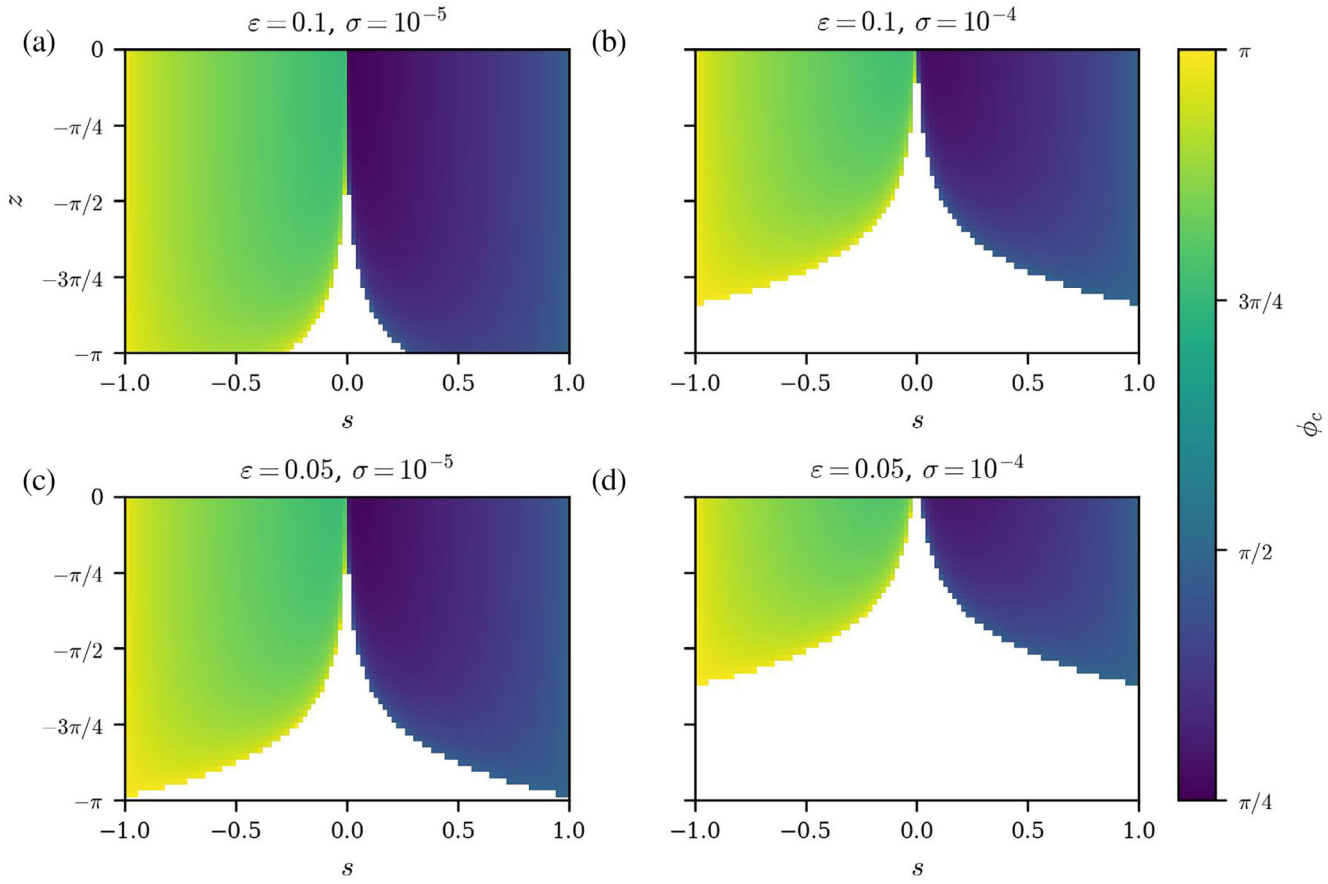

Fig. 2. Preferential zenith orientation, ϕ_c, of spheroid particles in waves and shear with various values of wave steepness (ε) and shear strength (σ): (**a**) $\varepsilon = 0.1$, $\sigma = 10^{-5}$; (**b**) $\varepsilon = 0.1$, $\sigma = 10^{-4}$; (**c**) $\varepsilon = 0.05$, $\sigma = 10^{-5}$; (**d**) $\varepsilon = 0.05$, $\sigma = 10^{-4}$. Regions with continually evolving orientation, that is, no ϕ_c, are indicated with no color.

given collection of particles and appropriate boundary conditions, the IOPs can be used to describe the light intensity within the collection of particles by solving the radiative transfer equation (Mishchenko 2014). However, this computation of the light intensity in the particulate medium is complicated by the light that is scattered by particles multiple times.

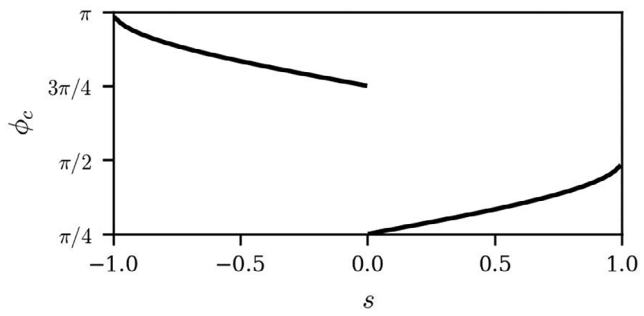

Fig. 3. Preferential zenith orientation, ϕ_c, of spheroid particles in waves (no shear). $s = 0$ are spheres, which have no orientation.

For simplicity, we ignore the multiple scattering of light and estimate the attenuation for monochromatic, unpolarized light by a collection of particles as (Bohren and Huffman 2004)

$$I(z) = I_i e^{-nC_e|z|} = I_i e^{-\tau} \tag{7}$$

where I is the light intensity in the particulate column, I_i is the incident light intensity, n is the particle concentration, C_e is the extinction cross section per particle, $|z|$ is the depth below the water surface, and $\tau = nC_e|z|$ is the optical depth. The only IOP required to calculate the optical depth is the extinction cross section, C_e, which is the sum of the scattering and absorption cross sections. While light intensity is in general a function of direction, that is., $I(\theta, \phi, \tau)$, this simplified model only considers unidirectional light within the context of single scattering. As such, it is accurate for a collection of particles with small total light attenuation, which is equivalent to an optically thin water column, that is, small τ.

To allow for variations with depth, z, a more general form of the optical depth, τ, is given by (Mishchenko 2014)

$$\tau(z) = \int_z^0 \sum_j C_{e,j} n_j(\zeta)\, d\zeta \tag{8}$$

where the subscript j indicates the particle type and ζ is a dummy variable for integrating over depth. The integrand is called the beam attenuation coefficient, $c = \sum C_e n$, which represents the bulk attenuation of a beam of light per unit depth in the water column.

There exists a variety of methods to estimate the optical cross sections of particles as a function of their shape, size, refractive index, and the wavelength of light in question. Numerically exact methods like the transfer matrix method can be used to find the IOPs for fixed and randomly oriented spheroids (Mishchenko 2000; Mishchenko and Travis 1998), but this method is limited to moderate optical sizes where the particle size and wavelength of light are comparable. On the other hand, the IOPs for particles that are large relative to the wavelength of light can be computed with the geometric optics approximation (Macke et al. 1995). For particle sizes where the IOPs can be calculated by neither the transfer matrix method nor geometric optics approximation, other approximate methods like the discrete dipole approximation can be used (Yurkin and Hoekstra 2011). Here, we will use a different approach, the AD approximation, which has the advantage of allowing for estimates of the optical cross sections (but not the phase function) of spheroids over a wide range of sizes (Shepelevich et al. 2001). Furthermore, for particles where the optical cross sections may be computed by both transfer matrix method and AD, the two methods give similar values (Clavano et al. 2007; Shepelevich et al. 2001).

Regardless of the method used, the optical cross section for a particle depends on the wavelength of light, the corresponding particle refractive index, and the particle size, shape, and orientation. We write the particle size using its volume-equivalent sphere radius $r_e = (r_d^2 r_l)^{1/3}$. The optical size of a particle is then given by $k_l r_e$ where $k_l = 2\pi/\lambda$ is the wavenumber for light and λ is the wavelength of light. The optical size describes the particle size relative to the wavelength of light. For light in the visible spectrum, particles of $r_e \gtrsim 1$ μm can be considered to be optically large ($k_l r_e \gtrsim 10$). Thus, many aquatic particles tend to be optically large (Stramski et al. 2004). The particle refractive index is written as $m = m_r + i m_i$, and is composed of real (m_r) and imaginary (m_i) parts. While the real part represents the difference in the propagation speed of light in the particle compared to the surrounding medium, the imaginary part represents the absorption of light by the particle. The refractive index is taken relative to water and depends on the wavelength of light and particle composition. Refractive index values are commonly close to $m = 1.05 + i0.01$ for organic aquatic particles and $m = 1.17 + i0.0001$ for inorganic aquatic particles (Clavano et al. 2007), and we use these as representative values below. Thus, the aquatic particles we consider tend to be optically soft, which is to say that the rates of light refraction and absorption are small relative to water (i.e., $|m-1|$ is small). Overall, aquatic particles meet the requirements for estimating the optical cross sections with the AD approximation: optically soft ($|m-1| \ll 1$) and optically large ($k_l r_e \gg 1$).

The extinction cross section for a spheroid with known size, shape, and orientation in the AD approximation is adapted from that for a sphere (Shepelevich et al. 2001), with

$$C_e = G Q_e \tag{9}$$

where $G = \pi r_d r_l \sqrt{1 + (a_r^{-2} - 1)\cos^2\phi}$ is the projected area of the spheroid oriented at zenith angle ϕ and Q_e is the extinction efficiency factor for a sphere (van de Hulst 1981)

$$\begin{aligned} Q_e(\rho,\beta) = 2 &- 4e^{-\rho\tan\beta}\left(\frac{\cos\beta}{\rho}\right)\sin(\rho-\beta) \\ &- 4e^{-\rho\tan\beta}\left(\frac{\cos\beta}{\rho}\right)^2\cos(\rho-2\beta) + 4\left(\frac{\cos\beta}{\rho}\right)^2\cos(2\beta). \end{aligned} \tag{10}$$

This factor represents the proportion of the extinction cross section to the projected area of the spheroid. Here, $\rho = 2k_l r_{oe}|m-1|$ is the phase delay parameter of the spheroid, representing the lag of light waves passing through the particle, with r_{oe} being the radius of an optically equivalent sphere given by

$$r_{oe} = \frac{r_d}{\sqrt{1 + (a_r^{-2} - 1)\cos^2\phi}} \tag{11}$$

Finally, the angle $\beta = \arctan(m_i/(m_r - 1))$ represents the strength of absorption relative to refraction. Thus, the extinction cross section for a spheroid with known size, shape, refractive index, and orientation can be found from Eqs. 9 to 11.

For randomly (isotropically) oriented spheroids, there is an optically equivalent distribution of spheres (Shepelevich et al. 2001)

$$f(\alpha) = \frac{a_r^{-4}\alpha_l^5}{(a_r^{-2} - 1)\alpha^5}\sqrt{\frac{a_r^{-2} - 1}{\alpha_d^2 - \alpha^2}} \tag{12}$$

where $\alpha_d = k_l r_d$ and $\alpha_l = k_l r_l$ are the optical sizes related to the spheroid and $\alpha = k_l r_{oe}$ is the optical size of the optically equivalent sphere of radius r_{oe}. The corresponding expected value of the extinction cross section is

$$C_{e,0} = \pi k_l^{-2}\int_{\alpha_l}^{\alpha_d} \alpha^2 Q_e(\rho = 2\alpha|m-1|;\beta) f(\alpha)\, d\alpha \tag{13}$$

where the subscript "0" indicates the random orientation case. This distribution of spheres has the same average volume and surface area as the spheroid particle, that is,

$$\frac{4\pi}{3}k_l^{-3}\int_{\alpha_l}^{\alpha_d}\alpha^3 f(\alpha)\,d\alpha=\frac{4\pi}{3}r_l r_d^2 \text{ and} \tag{14a}$$

$$4\pi k_l^{-2}\int_{\alpha_l}^{\alpha_d}\alpha^2 f(\alpha)\,d\alpha=2\pi r_d^2 S(a_r) \tag{14b}$$

where

$$S(a_r)=\begin{cases}1+a_r\dfrac{\arccos\left(a_r^{-1}\right)}{\sqrt{1-a_r^{-2}}} & a_r>1\\ 1+a_r\dfrac{\log\left(\sqrt{a_r^{-2}-1}+a_r^{-1}\right)}{\sqrt{a_r^{-2}-1}} & a_r<1\end{cases} \tag{15}$$

relates the spheroid's surface area to its equatorial cross section. Clavano et al. (2007) provide further description of the effect of spheroid size and shape on optical properties in the random orientation case.

Change in light attenuation due to preferential orientation

To isolate the change in light intensity due to preferential orientation, we consider the light intensity change relative to the random (isotropic) orientation case (Fig. 1c)

$$\Delta I=\frac{I}{I_0}=\frac{I_i e^{-\tau}}{I_i e^{-\tau_0}}=e^{-(\tau-\tau_0)}\,. \tag{16}$$

It is convenient to express the change in optical depth as

$$\tau-\tau_0=\overline{c}_0 z\left(\frac{\overline{c}}{\overline{c}_0}-1\right) \tag{17}$$

where

$$\overline{c}(z)=-\frac{1}{z}\int_z^0 c(\zeta)\,d\zeta \tag{18}$$

is the depth-averaged beam attenuation coefficient. We define

$$\Delta\overline{c}=\frac{\overline{c}}{\overline{c}_0}-1 \tag{19}$$

such that the change in light attenuation can be re-written as $\ln\Delta I=-\Delta\overline{c}\overline{c}_0 z$. For a given particle size, particle shape, particle refractive index, wavelength of light, and concentration profile, the change in light attenuation, ΔI, additionally depends on the random orientation beam attenuation coefficient, $\overline{c}_0$, and depth of interest, z. $\Delta\overline{c}$ represents the fractional change in the beam attenuation coefficient due solely to the preferential particle orientation induced by the flow condition (that can vary with depth). This allows us to focus on the importance of preferential orientation for particles of a given type.

If there is no current and the flow is dominated by waves, the preferential orientation does not depend on depth, and the change in beam attenuation coefficient for a given particle type can be simplified to

$$\overline{c}=C_e(\phi_c)\overline{n} \tag{20}$$

where $\overline{n}=-z^{-1}\int_z^0 n(\zeta)d\zeta$ is the depth-averaged concentration. The resulting relative change in beam attenuation coefficient is equivalent to the change in extinction cross section

$$\Delta\overline{c}=\frac{C_e(\phi_c)}{C_{e,0}}-1\,. \tag{21}$$

In the "Results" section, we use Eqs. 19 and 21 to evaluate the influence of preferential orientation on the beam attenuation coefficient in a wavy environment with and without shear, respectively.

Results

First, we consider the large particle limit in the case of $\rho=2k_l r_{\mathrm{oe}}\,|\,m-1\,|\to\infty$ where the results are simplified by $Q_e=2$. We then examine moderately sized particles that are optically large ($k_l r_{\mathrm{oe}}\gg 1$) but with finite phase delay parameter, creating size-dependent effects. Here, we use the term moderate to acknowledge that the smallest aquatic particles, like viruses and pico-phytoplankton, are too small for the AD approximation to apply.

Large particle limit

We first consider the case of $\rho\to\infty$, where particles are very large. In this limit the extinction efficiency factor (Eq. 10) reduces to $Q_e=2$, which is equivalent to the large particle efficiency found by Babinet's principle (van de Hulst 1981). Thus, the extinction cross section (Eq. 9) in the preferred orientation ($\phi=\phi_c$) simplifies to

$$C_e(\phi_c)=2G=2\pi r_d^2 a_r\sqrt{1+\left(a_r^{-2}-1\right)\cos^2\phi_c} \tag{22}$$

The extinction cross section for random (isotopic) orientation (Eq. 13) similarly simplifies to

$$C_{e,0}=2\pi k_l^{-2}\int_{\alpha_l}^{\alpha_d}\alpha^2 f(\alpha)\,d\alpha=\pi r_d^2 S(a_r) \tag{23}$$

which is the same result as found by taking $C_{e,0}=2G_0$ where G_0 is the average projected area of a randomly (isotopically) oriented convex particle (known to be one fourth its surface area, van de Hulst 1981).

We compute the change in attenuation coefficient due to waves and shear by inserting Eqs. 22 and 23 into Eq. 19, and assuming depth-uniform particle concentration ($n(z)=n_0$) to focus on orientation effects, to get

$$\Delta\bar{c}(z) = -\frac{2a_r}{S(a_r)}\frac{1}{z}\int_z^0 \sqrt{1+(a_r^{-2}-1)\cos^2\phi_c}\, dz - 1\,. \tag{24}$$

Using the previously found critical zenith angles, ϕ_c, from Eq. 5, we find

$$\Delta\bar{c}(z) = -\frac{2a_r}{S(a_r)}\frac{1}{z}\int_z^0 \sqrt{1-(a_r^{-2}-1)\frac{(s-1)(2s\varepsilon^2 e^{2\zeta}-\sigma)}{2s(\sigma+2\varepsilon^2 e^{2\zeta})}}\, d\zeta - 1 \tag{25}$$

which is valid for both oblate and prolate particle shapes.

When the flow is dominated by waves (i.e., no current), we can compute the change in attenuation coefficient by inserting Eqs. 22 and 23 into Eq. 21 and use Eq. 6 for the critical zenith angle to get

$$\Delta\bar{c} = \sqrt{2}\frac{a_r}{S(a_r)}\sqrt{1+s+\frac{1-s}{a_r^2}} - 1 \tag{26}$$

which is also valid for both oblate and prolate particle shapes. This is equivalent to taking $\sigma = 0$ in Eq. 25.

Figure 4a shows the relative change in beam attenuation coefficient up to the depth of wave-induced flow, $\Delta\bar{c}(z=-\pi)$, as a function of particle shape and dimensionless shear magnitude. This depth was chosen because wave motions are negligible below $z=-\pi$. We see that the influence of the shear is much weaker than that of particle shape. Fig. 4b shows the change in attenuation coefficient as a function of only the particle shape for wave-dominated flow (i.e., no current). Here, we see that, except a small decrease in attenuation coefficient for slightly prolate spheroids, $\Delta\bar{c}$ is positive and increases for more nonspherical shapes, suggesting that waves tend to increase light attenuation for large nonspherical particles.

The beam attenuation coefficient tends to increase in the wave preferred orientation because the particle's long axis tends to be aligned more horizontally, with this effect becoming stronger for larger aspect ratio particles. This results in a relatively large projected area among all possible orientations. This relative increase in projected area is greater for oblate spheroids than prolate because a flat disk more effectively increases the projected area than a horizontal rod. In other words, the larger value of $G(\phi_c)/G_0$ for oblate spheroids relative to prolate spheroids results in a larger value of $C_e(\phi_c)/C_{e,0}$ in the large size limit.

Moderately sized particles

For moderately sized particles, where particles are optically large ($k_l r_{oe} \gg 1$) but the phase delay parameter remains finite ($\rho \not\to \infty$), the extinction efficiency factor Q_e retains a dependence on particle size. In this case, the change in the beam attenuation coefficient depends on particle size, shape and refractive index. But, given that we found that $\Delta\bar{c}(z=-\pi)$ only exists for small shear strengths that only weakly influence the orientation of the particles, we neglect shear and focus on the case where waves dominate the flow.

To incorporate the effect of size, we can rewrite the change in beam attenuation coefficient as

$$\Delta\bar{c} = \frac{G}{G_0}\frac{Q_e(\rho,\beta)}{Q_{e,0}} - 1 = \frac{a_r}{2S(a_r)}\sqrt{1+(a_r^{-2}-1)\cos^2\phi}\frac{Q_e(\rho,\beta)}{Q_{e,0}} - 1 \tag{27}$$

where $Q_{e,0} = C_{e,0}/G_0$. The ratio of extinction efficiency in the wave preferred and random orientations encapsulates the size

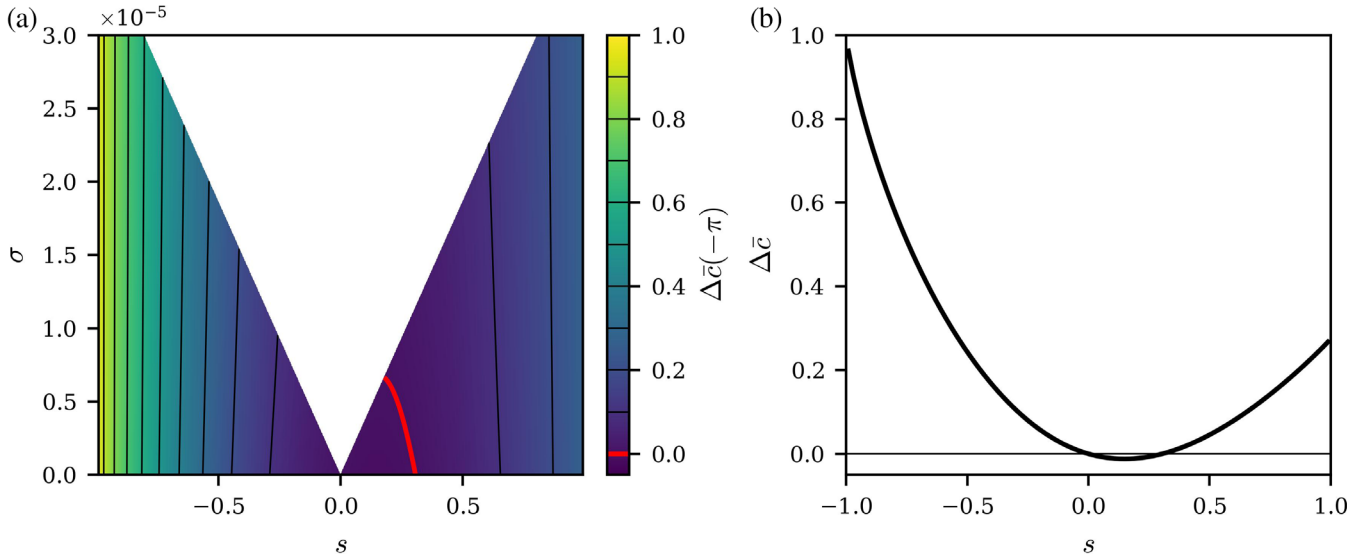

Fig. 4. Change in attenuation coefficient in the large particle limit ($\rho \to \infty$) due to preferential orientation: (**a**) waves and shear flow (Eq. 25) evaluated at $z=-\pi$; and (**b**) waves only flow (Eq. 26). No color in panel a represents no solution for ϕ_c. Panel b is the $\sigma = 0$ transect from (**a**).

dependency since G/G_0 is independent of size. Note, taking $Q_e = Q_{e,0}$ reverts to the results for the large particle size limit.

The influence of particle size and orientation is introduced through the phase delay parameter, ρ, and how it affects the extinction efficiency factor, $Q_e(\rho, \beta)$. The resulting change in attenuation coefficient due to wave preferred orientation must be computed via numerical integration; we use the composite Simpson's rule. The phase delay parameter varies from $2\alpha_l\,|\,m-1\,|$ to $2\alpha_d\,|\,m-1\,|$ in the random orientation case, so the corresponding particle size to it's ρ value is found from Eq. 11.

In Fig. 5, we observe that particles with small phase delay parameters tend to decrease the beam attenuation coefficient in the wave-preferred orientation, while particles with larger phase delay parameters tend to increase it. This is due to contrasting behavior of how extinction efficiency varies with orientation when ρ is small or large. A particle with sufficiently large ρ has an extinction efficiency of approximately 2 regardless of orientation. Consequently, the orientation with the largest projected area, that is, the long axis aligned perpendicular to the optical axis, has the largest extinction cross section. In contrast, for $\rho \lesssim 2$, Q_e increases monotonically with ρ such that the orientation with the long axis aligned with the optical axis (vertical) tends to have the largest Q_e, since ρ is proportional to the distance light travels through the particle. Q_e increases rapidly with ρ when ρ is small due to destructive scattering patterns that contribute to attenuation. When ρ is large both destructive and constructive scattering patterns contribute, leading to oscilatory values of Q_e. The rapid increase in Q_e with ρ results in a maximum C_e in the orientation with the maximum path length for light through the particle, even though the projected area is reduced in this orientation. Since the flow tends to orient the particles' long axis toward the horizontal direction, the resulting flow-aligned beam attenuation coefficient tends to decrease for small ρ particles, whereas it tends to increase for large ρ particles.

The results are more sensitive to particle size and shape for non-absorbing particles ($\beta = 0^\circ$) than for absorbing particles ($\beta = 10^\circ$). This sensitivity arises from strong oscillations in Q_e with ρ. As $\rho \to \infty$, $Q_e \to 2$ with decaying oscillations for all β values, but the oscillations decay more slowly for small β. This can be understood by considering the relative contributions of scattering and absorption to extinction. With β representing the relative strength of absorption vs. refraction, increases in β give greater weight to absorption and damp the oscillations in the extinction efficiency faster. Additionally, the phase delay parameter depends on particle orientation, so slight changes between fixed and random orientations affect the beam attenuation coefficient. The direction of change in extinction efficiency can reverse if Q_e is near a peak while $Q_{e,0}$ is near a trough, or vice versa. These behaviors are evident for nearly spherical particles ($|\,s\,| \ll 1$) in Fig. 5a. For strongly nonspherical particles ($|\,s\,| \sim 1$), variations are dominated by shape, similar to the large size limit, but oscillate in magnitude. These results are explored further in the examples in the "Applications" section.

Applications

To understand the implications of our results for the beam attenuation coefficient in aquatic environments, we now consider the application of our idealized modeling framework to particles with properties that are representative of bacteria, algae, and microplastics.

Organic vs. inorganic particles

Following Clavano et al. (2007), we first split particles into two representative refractive indices: $m = 1.17 + i0.0001$ for inorganic particles and $m = 1.05 + i0.01$ for organic particles. The inorganic refractive index is representative of some

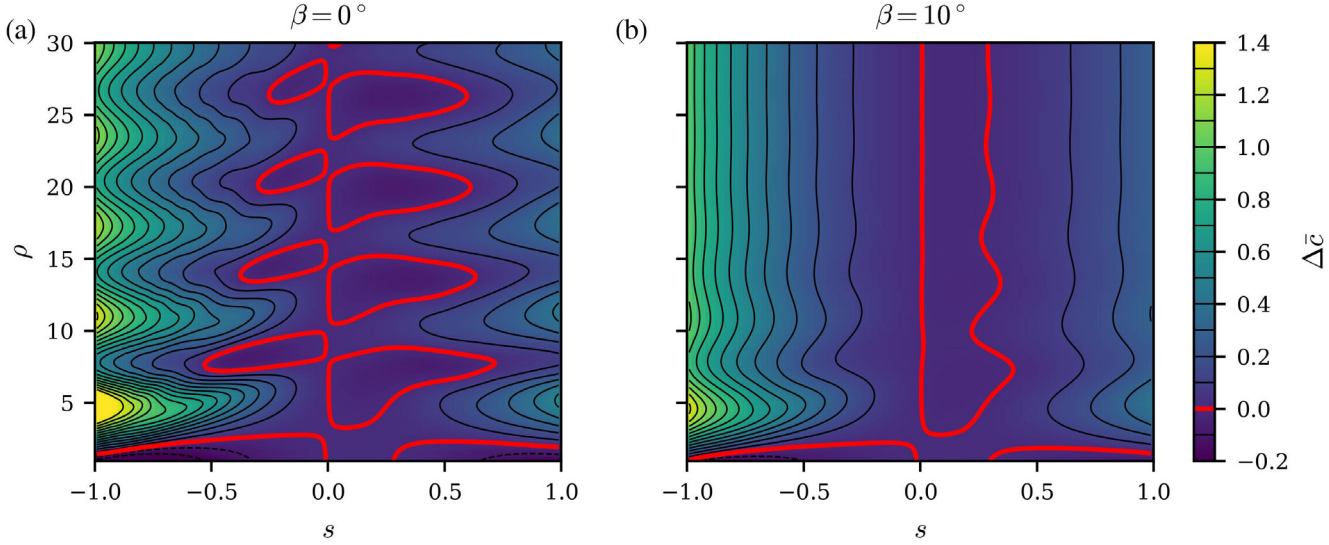

Fig. 5. Change in attenuation coefficient for wave-dominated flow (i.e., no current) for moderately sized particles: (**a**) non-absorbing particle ($\beta = 0^\circ$); and (**b**) absorbing particle ($\beta = 10°$). Figure 4b corresponds approximately to data along $\rho = 30$ in (**b**).

plastics (e.g., polyethylene that has $m_r \approx 1.13$ at a wavelength of $\lambda = 589$ nm, Cardarelli 2008) as well as naturally occurring inorganic particles such as minerals. The organic refractive index is representative of living cells such as bacteria or algae. Note, the real parts of m are relative to the refractive index of water in a vacuum ($m_r \approx 1.33$). The refractive index enters the problem via the phase delay parameter, $\rho = 2k_l r_{\mathrm{oe}} |m - 1|$, and thus influences the extinction efficiency (Fig. 1b, Eq. 10) along with the particle size and wavelength of light.

Figure 6 shows the change in beam attenuation coefficient for the representative organic and inorganic particles of varying size and shape due to preferential orientation in waves (i.e., no current) at the wavelength of light corresponding to the red peak absorbance band of chlorophyll a (Chl *a*) ($\lambda = 676$ nm). Inorganic particles exhibit a strong variation of $\Delta\bar{c}$ in both particle shape and particle size (Fig. 6a), including changes in sign of $\Delta\bar{c}$ and a large relative increase in $\Delta\bar{c}$ for small, highly oblate particles. The variations with particle size come from the larger refractive index, whereas the variations with particle shape come from the small value of β, since the extinction cross section is more sensitive to the value of ρ when $\beta \approx 0$ (Fig. 5a). These results for moderately sized inorganic particles contrast those for particles in the large size limit, where it was observed that the attenuation coefficient almost always increases in the wave preferred orientation, with the exception of very weakly prolate particle shapes (Fig. 4).

Organic particles exhibit a more gradual variation of $\Delta\bar{c}$ in shape and size compared to the inorganic case (Fig. 6b). The smaller refractive index implies that ρ varies modestly with particle size. Nonspherical particles with $D_e \lesssim 5$ μm generally decrease the attenuation coefficient, except for some slightly prolate spheroids. Moreover, the absorbing component (the comparatively larger value of β) means that the organic particles reach the large size limit at a smaller dimensional size relative to inorganic particles. Together, these features suggest that small nonspherical organic particles such as bacteria decrease the attenuation coefficient, but larger nonspherical particles like algae tend to increase the attenuation coefficient in the wave preferred orientation.

Escherichia coli, diatoms, and microplastics

To our knowledge, the influence of wave preferred particle alignment on the light climate in water columns has not been previously studied, but the effect of shear flows in the ocean has received some attention. In particular, Marcos et al. (2011) examined the light attenuation due to the orientation of bacteria (*E. coli*) in a laboratory-generated shear flow device, and McFarland et al. (2020) examined the light attenuation due to the orientation of diatom (phytoplankton) colonies (*Ditylum. brightwellii*) in the field in the presence of a sheared current. Both particles have elongated prolate shapes, which in shear flows tend to align with their longest axis being horizontal.

Table 1 gives the change in beam attenuation coefficient for such particles in waves in our framework, where the preferred orientation is also close to the longest particle axis being horizontal. We observe qualitative agreement between our results and those in Marcos et al. (2011) (who reported a 13% decrease in scattering cross section for bacteria) and McFarland et al. (2020) (who reported an increase in absorption attenuation coefficient of up to 24.5% for diatom colonies) due to the similarity in the preferred orientations, although they use different methods. Due to the reasons outlined above, while wave-aligned bacteria decrease the beam

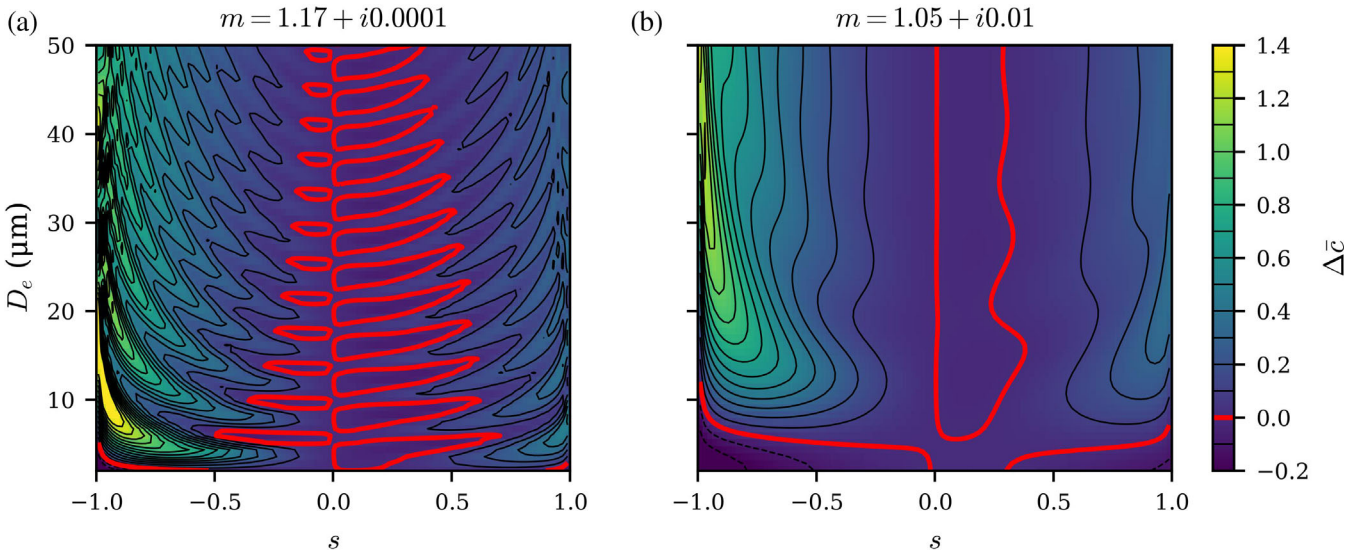

Fig. 6. Change in attenuation coefficient for the waves only scenario, for particles with equivalent volume sphere diameters, $D_e = 2r_e$, ranging from 2 to 50 μm with $\lambda = 676$ nm: (**a**) refractive index representing inorganic particle, (**b**) refractive index representing organic particle in peak absorbance band.

Table 1. Change in beam attenuation coefficient for representative particles in wave preferred orientations. Organic particles are computed with $\lambda = 676$ nm, microplastics with $\lambda = 589$ nm.

Particle	Diameter (μm)	Length (μm)	Refractive index	$\Delta\bar{c}$
Escherichia coli bacteria	1.1	3.5	1.05	−0.19
Diatom (*Ditylum brightwellii*) colony	50	800	$1.035 + i0.00056$	0.31
Plate-like microplastic	1000	200	$1.17 + i0.0001$	0.80
Rod-like microplastic	200	1000	$1.17 + i0.0001$	0.24

attenuation coefficient, wave-aligned diatom colonies increase it.

Table 1 also gives results for particles of sizes and shapes typical of two different microplastics found in the ocean (Cózar et al. 2014). While plastic particles can take on a variety of shapes, they can be grouped into limiting values such as plate-like and rod-like (Contreras et al. 2024). For both typical plate-like and rod-like microplastics, we find that the attenuation coefficient at a non-absorbing wavelength is significantly increased due to wave-induced preferred alignment.

Lake algal bloom

We finally consider the effect of waves and shear on the light attenuation by a cyanobacterium that may be the dominant particle type during lake blooms. Taking Lake Mendota (Wisconsin, USA) as an example, we consider a hypothetical bloom of the rod-shaped cyanobacterium *Synechococcus* with a length of 20 μm and diameter of 10 μm (corresponding to $D_e = 12.6$ μm, $a_r = 2$, and $s = 0.6$), and refractive index $m = 1.05 + i0.01$ (representative of organic aquatic particles corresponding to the red peak absorbance band of Chl *a*). We assign a representative concentration profile of $n(z) = n_0 e^{az}$, where $n_0 = 10^9$ cells m^{-3} (i.e., 1000 cells per mL) at the water surface and the concentration decays with depth at a rate of $a = 5$ m^{-1}. This taxon and concentration are in the range of bloom concentrations observed on Lake Mendota (Magnuson et al. 2022). By considering the attenuation with and without flow-induced preferential orientation, we quantify how the beam attenuation coefficient changes due to a sudden onset of waves and a sheared current by a wind event. On Lake Mendota, a wind event that occurs during such a bloom might result in waves of height 10 cm and period 1.5 s in water depth of 15 m, which results in wave-induced flow motions that align particles up to a depth of about 2 m. The corresponding wind-generated surface current in the water might have a shear of magnitude $\sigma = 10^{-4}$ s^{-1}.

Figure 7 shows the results for this situation. The beam attenuation coefficients in flow preferred orientation and random (isotropic) orientation (Fig. 7b) show that there is an increase in the beam attenuation coefficient due to the preferential orientations of the cells. The fractional change in the beam attenuation coefficient in this case is an approximate 14%–24% increase (Fig. 7c) so that flow-aligned cyanobacterial cells allow less light to penetrate the upper water column. This occurs because the preferential orientation increases the particle extinction cross section, which results in a larger $c = C_e n$ at a given depth. The influence of shear is small compared to that of waves near the surface but results in an increase in $\Delta\bar{c}$ at larger depths.

Discussion

We have constructed an idealized model for examining the effect of preferential particle orientation in waves and shear

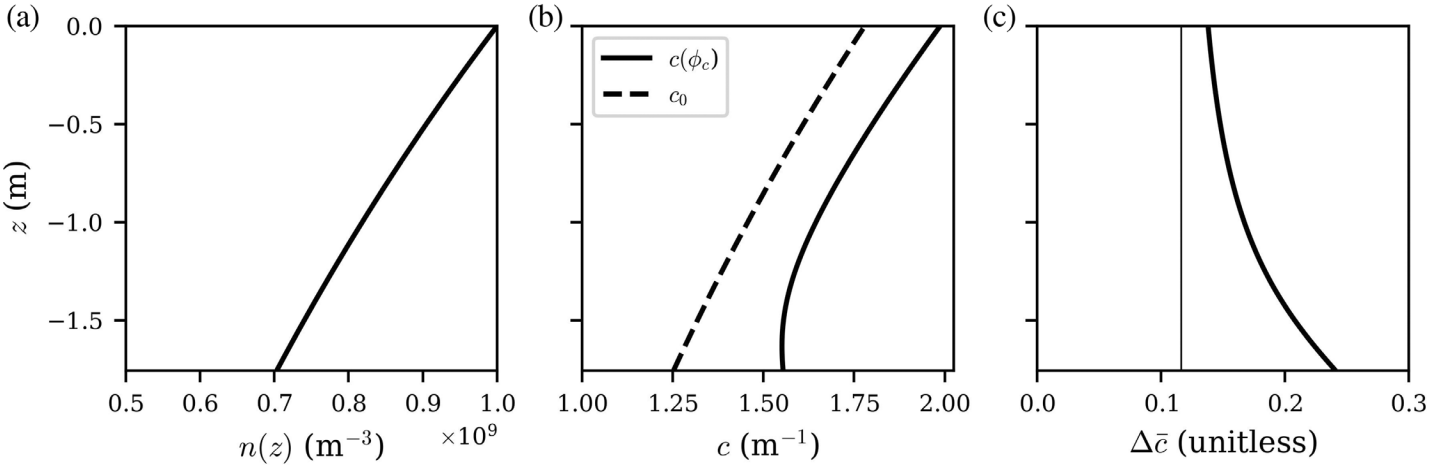

Fig. 7. Example of change in beam attenuation coefficient due to *Synechococcus* in waves and shear where $\varepsilon = 0.178$ and $\sigma = 5.6\ 10^{-5}$; the particle has a length of 20 μm, diameter of 10 μm (corresponding to $D_e = 12.6$ μm and $s = 0.6$), and $m = 1.05 + i0.01$; the concentration profile decays exponentially with a mixing length scale of 5 m: (**a**) concentration profile, (**b**) variation of attenuation coefficient with elevation in preferential and random orientation, (**c**) depth averaged change in beam attenuation coefficient; (**c**) has a thin black line that represents $\sigma = 0$ to emphasize the contribution of shear.

flow on light attenuation in the water column through the beam attenuation coefficient. To do this, we have made simplifying assumptions, both in terms of the orientation dynamics and the optical properties. Here, we discuss limitations and implications of some of these assumptions before reiterating the main results from our idealized model.

The particle orientation dynamics neglect the effects of wave–current interactions, inertial effects in fluid–particle interactions, particle buoyancy, and other complications like random (turbulent) flow variations. For the larger particles we consider (e.g., algae and microplastics), inertial effects in fluid–particle interactions are expected to lead toward a stronger preference for the particles' long axis being horizontal (Dabade et al. 2015; DiBenedetto et al. 2019; Rosén et al. 2015). Additionally, the concentration profile for buoyant particles can be modified by waves (DiBenedetto 2020). Finally, for some organic particles (e.g., cell colonies) or pollutants (e.g., flexible fibers), the particles' flexibility can mean that their shape and orientation evolve with the flow (Gay et al. 2018; Verhille 2022). The simplified orientation modeling used herein does not include any of these effects, but rather it gives an idealized representation of the preferential orientation particles exhibit in waves and shear flow.

The optical model computes the attenuation of an idealized case of vertically oriented, monochromatic, unpolarized, beam of light by optically soft homogeneous spheroid particles. We assume that the particles are optically large (i.e., $D_e \gtrsim 1$ μm), which is true for many aquatic particles, but some exceptions include viruses and pico-phytoplankton (Stramski et al. 2004). The assumption of optically homogeneous spheroids is not the case for actual organic particles which can be non-homogeneous cells, that is, their optical properties vary within the sub-cell components, or are composed of many individual cells as a colony. More comprehensive optical models may be obtained by considering coated spheres (Lehmuskero et al. 2018) or sphere lattices (Zhai et al. 2020).

The assumption of monochromatic light requires recomputing the change in beam attenuation coefficient for different wavelengths of light. It would be interesting to use such results to extract spectral effects commonly considered in remote sensing applications. The large particle limit results ("Large particle limit" section) are not sensitive to changes in λ or m, whereas for moderate sizes, small changes to the phase delay parameter, ρ, or the relative effect of absorption, β, could vary the outcome significantly (Fig. 5), assuming the optically soft requirement holds for all wavelengths considered. Moreover, the simplified geometry of our model neglects the multiple scattering of light that is known to influence the light climate when scattering particle concentrations are high (Rose 2024), which may be the case in bloom conditions.

Our approach of coupling simplified particle orientation and optical models demonstrates the significance of preferential particle orientation by waves and sheared flow on the beam attenuation coefficient in an idealized water column. In the large limit, that is, $D_e \gtrsim 400$ μm for a particle that does not absorb light and $D_e \gtrsim 50$ μm for an absorbing particle, particles tend to enhance the beam attenuation coefficient. This is because they expose a larger area to light in their preferred flow orientation compared to the random case, and this effect is dependent on particle shape. For moderate particle sizes, that is, particles with $D_e \gtrsim 1$ μm but smaller than the large size limit, the change in beam attenuation coefficient varies with both size and shape.

Interestingly, in the wave-aligned orientation, small particles ($1 \lesssim D_e \lesssim 10$ μm, e.g., bacteria) tend to decrease the beam attenuation coefficient, while larger particles ($D_e \gtrsim 10$ μm, e.g., algae) tend to increase it. This size-dependent behavior arises from a difference in how attenuation efficiency varies with orientation. Small particles ($1 \lesssim D_e \lesssim 10$ μm) tend to attenuate the most light when their long axis aligns with the direction of light (vertical), even though the particle has a smaller projected area. Conversely, for larger particles ($D_e \gtrsim 10$ μm), the orientation with the largest area exposed to light tends to attenuate the most light. Waves and shear flow align the long axis of particles horizontally, resulting in a small attenuation for small particles and a large attenuation for large particles compared to the random (isotropic) orientation. The estimated increase in the beam attenuation coefficient is approximately 10–25% for particles the size of algae or microplastics, while bacteria-sized particles tend to decrease the beam attenuation coefficient by approximately 10–20%.

Our results indicate that preferential alignment can significantly influence the inherent optical properties of aquatic particles in a wavy environment. The resulting change may influence ecosystem processes by increasing the light available to particles near the surface or by occluding the light beneath them. We expect that this framework can be used to help analyze in situ light climates with wave-aligned particles, but laboratory and field work should be performed to ensure our simple model yields reliable predictions across a wide range of conditions. Given the importance of geometry and directional scattering in comprehensive light attenuation models, future work should also consider the influence of multiple scattering in the water column.

Author Contributions

Samuel T. Salemink-Harry: conceptualization, data curation, formal analysis, methodology, software, validation, visualization, writing – original draft preparation, writing – review and editing. Benjamin J. Smith: formal analysis, methodology, validation, writing – original draft preparation, writing – review and editing. Hilary A. Dugan: funding acquisition, writing – review and editing. Jennifer A. Franck: funding acquisition, resources, writing – review and editing. Till J. W. Wagner: funding acquisition, writing – review and editing. Lucas K. Zoet: funding acquisition, writing – review and editing. Grace M. Wilkinson: formal analysis, funding acquisition,

validation, writing – review and editing. Nimish Pujara: conceptualization, formal analysis, funding acquisition, methodology, project administration, resources, supervision, validation, writing – original draft preparation, writing – review and editing.

Acknowledgments

Support for this research was provided by the University of Wisconsin–Madison Office of the Vice Chancellor for Research with funding from the Wisconsin Alumni Research Foundation. Wilkinson was also supported by NSF DEB #2025982. Pujara was also supported by NSF CBET #2338221 and an Early-Career Research Fellowship from the Gulf Research Program of the National Academies of Sciences, Engineering, and Medicine.

Conflicts of Interest

None declared.

Data Availability Statement

The code used to generate the data presented here is openly available at the Zenodo research repository https://doi.org/10.5281/zenodo.16895121.

References

Bickmore, B. R., K. L. Nagy, P. E. Sandlin, and T. S. Crater. 2002. "Quantifying Surface Areas of Clays by Atomic Force Microscopy." *American Mineralogist* 87, no. 5–6: 780–783. https://doi.org/10.2138/am-2002-5-622.

Bohren, C. F., and D. R. Huffman. 2004. Absorption and Scattering of Light by Small Particles. Wiley-CH Verlag GmbH & Co KGaA. https://doi.org/10.1002/9783527618156.

Bricaud, A., H. Claustre, J. Ras, and K. Oubelkheir. 2004. "Natural Variability of Phytoplanktonic Absorption in Oceanic Waters: Influence of the Size Structure of Algal Populations." *Journal of Geophysical Research: Oceans* 109, no. C11: 2004JC002419. https://doi.org/10.1029/2004JC002419.

Cardarelli, F. 2008. Materials Handbook: A Concise Desktop Reference. Springer.

Clavano, W., E. Boss, and L. Karp-Boss. 2007. "Inherent Optical Properties of Non-Spherical Marine-like Particles—From Theory to Observation." In Oceanography and Marine Biology, edited by R. Gibson, R. Atkinson, and J. Gordon, vol. 20074975, 1–38. CRC Press. https://doi.org/10.1201/9781420050943.ch1.

Contreras, L., C. Edo, and R. Rosal. 2024. "Mass Concentration of Plastic Particles From Two-Dimensional Images." *Science of the Total Environment* 946: 173849. https://doi.org/10.1016/j.scitotenv.2024.173849.

Cózar, A., F. Echevarría, J. I. González-Gordillo, et al. 2014. "Plastic Debris in the Open Ocean." *Proceedings of the National Academy of Sciences of the United States of America* 111, no. 28: 10239–10244. https://doi.org/10.1073/pnas.1314705111.

Dabade, V., N. K. Marath, and G. Subramanian. 2015. "Effects of Inertia and Viscoelasticity on Sedimenting Anisotropic Particles." *Journal of Fluid Mechanics* 778: 133–188. https://doi.org/10.1017/jfm.2015.360.

Dean, R. G., and R. A. Dalrymple. 1991. Water Wave Mechanics for Engineers and Scientists. Vol. 2. World Scientific Publishing Co. https://doi.org/10.1142/1232.

DiBenedetto, M. H., N. T. Ouellette, and J. R. Koseff, 2017. Transport of Anisotropic Particles Under Waves. Journal of Fluid Mechanics, 837: 320–340. https://doi.org/10.1017/jfm.2017.853.

DiBenedetto, M. H. 2020. "Non-Breaking Wave Effects on Buoyant Particle Distributions." *Frontiers in Marine Science* 7: 148. https://doi.org/10.3389/fmars.2020.00148.

DiBenedetto, M. H., J. R. Koseff, and N. T. Ouellette. 2019. "Orientation Dynamics of Nonspherical Particles Under Surface Gravity Waves." *Physical Review Fluids* 4, no. 3: 034301. https://doi.org/10.1103/physrevfluids.4.034301.

DiBenedetto, M. H., and N. T. Ouellette. 2018. "Preferential Orientation of Spheroidal Particles in Wavy Flow." *Journal of Fluid Mechanics* 856: 850–869. https://doi.org/10.1017/jfm.2018.738.

Font-Muñoz, J. S., R. Jeanneret, I. Tuval, and G. Basterretxea. 2020. "Method for the Determination of Preferential Orientation of Marine Particles From Laser Diffraction Measurements." *Optics Express* 28, no. 9: 14085–14099. https://doi.org/10.1364/OE.390388.

Gay, A., B. Favier, and G. Verhille. 2018. "Characterisation of Flexible Fibre Deformations in Turbulence." *EPL (Europhysics Letters)* 123, no. 2: 24001. https://doi.org/10.1209/0295-5075/123/24001.

Jeffery, G. B. 1922. "The Motion of Ellipsoidal Particles Immersed in a Viscous Fluid." *Proceedings of the Royal Society of London. Series A, Containing Papers of a Mathematical and Physical Character* 102, no. 715: 161–179. https://doi.org/10.1098/rspa.1922.0078.

Johnson, G. C., B. M. Sloyan, W. S. Kessler, and K. E. McTaggart. 2002. "Direct Measurements of Upper Ocean Currents and Water Properties Across the Tropical Pacific during the 1990s." *Progress in Oceanography* 52, no. 1: 31–61. https://doi.org/10.1016/S0079-6611(02)00021-6.

Jonasz, M., and G. Fournier. 2007. "Light Scattering by Particles in Water." In Theoretical and Experimental Foundations. Elsevier. https://doi.org/10.1016/B978-0-12-388751-1.X5000-5.

Lehmuskero, A., M. Skogen Chauton, and T. Boström. 2018. "Light and Photosynthetic Microalgae: A Review of Cellular- and Molecular-Scale Optical Processes." *Progress in Oceanography* 168: 43–56. https://doi.org/10.1016/j.pocean.2018.09.002.

Ma, K., N. Pujara, and J.-L. Thiffeault 2022. Reaching for the Surface: Spheroidal Microswimmers in Surface Gravity Waves. Physical Review Fluids 7(1): 014310. https://doi.org/10.1103/physrevfluids.7.014310.

Macke, A., M. I. Mishchenko, K. Muinonen, and B. E. Carlson. 1995. "Scattering of Light by Large Nonspherical Particles: Ray-Tracing Approximation Versus T-Matrix Method." *Optics Letters* 20, no. 19: 1934–1936. https://doi.org/10.1364/OL.20.001934.

Magnuson, J. J., S. R. Carpenter, and E. H. Stanley. 2022. North Temperate Lakes LTER: Phytoplankton – Madison Lakes Area 1995 – Current. Environmental Data Initiative. https://doi.org/10.6073/PASTA/BD03330E83FC52A5442BB39E131C95E9.

Marcos, J. R. Seymour, M. Luhar, et al. 2011. "Microbial Alignment in Flow Changes Ocean Light Climate." *Proceedings of the National Academy of Sciences of the United States of America* 108, no. 10: 3860–3864. https://doi.org/10.1073/pnas.1014576108.

McFarland, M., A. R. Nayak, N. Stockley, M. Twardowski, and J. Sullivan. 2020. "Enhanced Light Absorption by Horizontally Oriented Diatom Colonies." *Frontiers in Marine Science* 7: 494. https://doi.org/10.3389/fmars.2020.00494.

Mishchenko, M. I. 2000. "Calculation of the Amplitude Matrix for a Nonspherical Particle in a Fixed Orientation." *Applied Optics* 39, no. 6: 1026–1031. https://doi.org/10.1364/AO.39.001026.

Mishchenko, M. I. 2014. Electromagnetic Scattering by Particles and Particle Groups: An Introduction. 1st ed. Cambridge University Press. https://doi.org/10.1017/CBO9781139019064.

Mishchenko, M. I., and L. D. Travis. 1998. "Capabilities and Limitations of a Current FORTRAN Implementation of the T-Matrix Method for Randomly Oriented, Rotationally Symmetric Scatterers." *Journal of Quantitative Spectroscopy and Radiative Transfer* 60, no. 3: 309–324. https://doi.org/10.1016/S0022-4073(98)00008-9.

Mishchenko, M. I., L. D. Travis, and A. A. Lacis. 2002. Scattering, Absorption, and Emission of Light by Small Particles. Cambridge University Press.

Mobley, C., E. Boss, and C. Roesler. 2020. Ocean Optics Web Book. International Ocean Colour Coordinating Group.

Nayak, A. R., E. Malkiel, M. N. McFarland, M. S. Twardowski, and J. M. Sullivan. 2021. "A Review of Holography in the Aquatic Sciences: In Situ Characterization of Particles, Plankton, and Small Scale Biophysical Interactions." *Frontiers in Marine Science* 7: 572147. https://doi.org/10.3389/fmars.2020.572147.

Noel, V., and H. Chepfer. 2004. "Study of Ice Crystal Orientation in Cirrus Clouds Based on Satellite Polarized Radiance Measurements." *Journal of the Atmospheric Sciences* 61, no. 16: 2073–2081. https://doi.org/10.1175/1520-0469(2004)061<2073:SOICOI>2.0.CO;2.

Pujara, N., J.-A. Arguedas-Leiva, C. C. Lalescu, B. Bramas, and M. Wilczek. 2021. "Shape- and Scale-Dependent Coupling Between Spheroids and Velocity Gradients in Turbulence." *Journal of Fluid Mechanics* 922: R6. https://doi.org/10.1017/jfm.2021.543.

Pujara, N., and J.-L. Thiffeault. 2023. "Wave-Averaged Motion of Small Particles in Surface Gravity Waves: Effect of Particle Shape on Orientation, Drift, and Dispersion." *Physical Review Fluids* 8, no. 7: 074801. https://doi.org/10.1103/PhysRevFluids.8.074801.

Rose, K. C. 2024. "Light in Inland Waters." In Wetzel's Limnology, 75–94. Elsevier. https://doi.org/10.1016/B978-0-12-822701-5.00006-9.

Rosén, T., M. Do-Quang, C. K. Aidun, and F. Lundell. 2015. "Effect of Fluid and Particle Inertia on the Rotation of an Oblate Spheroidal Particle Suspended in Linear Shear Flow." *Physical Review E* 91, no. 5: 053017. https://doi.org/10.1103/physreve.91.053017.

Ross, M. R. V., S. N. Topp, A. P. Appling, et al. 2019. "AquaSat: A Data Set to Enable Remote Sensing of Water Quality for Inland Waters." *Water Resources Research* 55, no. 11: 10012–10025. https://doi.org/10.1029/2019WR024883.

Seo, K. W., H. J. Byeon, and S. J. Lee. 2014. "Measuring the Light Scattering and Orientation of a Spheroidal Particle Using in-Line Holography." *Optics Letters* 39, no. 13: 3915–3918. https://doi.org/10.1364/OL.39.003915.

Shepelevich, N. V., I. V. Prostakova, and V. N. Lopatin. 2001. "Light-Scattering by Optically Soft Randomly Oriented Spheroids." *Light Scattering by Non-Spherical Particles* 70, no. 4: 375–381. https://doi.org/10.1016/S0022-4073(01)00017-6.

Shulman, M. D., and R. A. Bryson. 1961. "The Vertical Variation of Wind-Driven Currents in Lake Mendota1." *Limnology and Oceanography* 6, no. 3: 347–355. https://doi.org/10.4319/lo.1961.6.3.0347.

Stramski, D., E. Boss, D. Bogucki, and K. J. Voss. 2004. "The Role of Seawater Constituents in Light Backscattering in the Ocean." *Progress in Oceanography* 61, no. 1: 27–56. https://doi.org/10.1016/j.pocean.2004.07.001.

van de Hulst, H. C. 1981. "Light Scattering by Small Particles." Dover Publications.

Ventrella, F. M., N. Pujara, G. Boffetta, M. Cencini, J.-L. Thiffeault, and F. De Lillo. 2023. "Microswimmer Trapping in Surface Waves with Shear." *Proceedings of the Royal Society A: Mathematical, Physical and Engineering Sciences* 479, no. 2278: 20230280. https://doi.org/10.1098/rspa.2023.0280.

Verhille, G. 2022. "Deformability of Discs in Turbulence." *Journal of Fluid Mechanics* 933: A3. https://doi.org/10.1017/jfm.2021.1035.

Voth, G. A., and A. Soldati. 2017. "Anisotropic Particles in Turbulence." *Annual Review of Fluid Mechanics* 49, no. 1: 249–276. https://doi.org/10.1146/annurev-fluid-010816-060135.

Werdell, P. J., L. I. McKinna, E. Boss, et al. 2018. "An Overview of Approaches and Challenges for Retrieving Marine Inherent Optical Properties From Ocean Color Remote Sensing." *Progress in Oceanography* 160: 186–212. https://doi.org/10.1016/j.pocean.2018.01.001.

Wu, T., B. Qin, W. Ding, et al. 2018. "Field Observation of Different Wind-Induced Basin-Scale Current Field Dynamics in a Large, Polymictic, Eutrophic Lake." *Journal of Geophysical Research: Oceans* 123, no. 9: 6945–6961. https://doi.org/10.1029/2018JC014040.

Yurkin, M. A., and A. G. Hoekstra. 2011. "The Discrete-Dipole-Approximation Code ADDA: Capabilities and Known Limitations." *Journal of Quantitative Spectroscopy and Radiative Transfer* 112, no. 13: 2234–2247. https://doi.org/10.1016/j.jqsrt.2011.01.031.

Zhai, S., M. Twardowski, J. D. Hedley, M. McFarland, A. R. Nayak, and T. Moore. 2020. "Optical Backscattering and Linear Polarization Properties of the Colony Forming Cyanobacterium Microcystis." *Optics Express* 28, no. 25: 37149–37166. https://doi.org/10.1364/OE.405871.

Zhao, L., and H. I. Andersson. 2016. "Why Spheroids Orient Preferentially in near-Wall Turbulence." *Journal of Fluid Mechanics* 807: 221–234. https://doi.org/10.1017/jfm.2016.619.*Submitted 08 April 2025*

Revised 18 August 2025

Accepted 29 September 2025